Check for updates

ADVANCED OPTICAL MATERIALS
www.advopticalmat.de

Spintronic Terahertz Emission in Ultrawide Bandgap Semiconductor/Ferromagnet Heterostructures

Andrew Comstock, Melike Biliroglu, Dovletgeldi Seyitliyev, Aeron McConnell, Eric Vetter, Pramod Reddy, Ronny Kirste, Dennis Szymanski, Zlatko Sitar, Ramón Collazo, Kenan Gundogdu, and Dali Sun**

Recent successful integration of semiconductors into spintronic THz emitters has demonstrated a new pathway of control over terahertz (THz) radiation through ultrafast demagnetization dynamics. Here, the spintronic THz emission from different ultrawide bandgap (UWBG) semiconductors interfaced with ferromagnets is studied. The authors show that the Schottky barrier in the UWBG semiconductor AlN acts as a spin filter that increases the polarization of the spin current injected from the ferromagnet. Furthermore, the authors show that the two-dimensional electron gas at the interface between $Al_{0.25}Ga_{0.75}N$ and GaN enhances the magnitude of the emitted radiation due to the high spin-to-charge conversion efficiency induced by the Rashba effect that results in a hallmark asymmetry in emission amplitude. The results provide a framework for future engineering of semiconducting/ferromagnet heterostructures for ultrafast communications technologies beyond 5G.

1. Introduction

Electromagnetic radiation with frequencies extending into the terahertz (THz) regime is of immense technological importance for high-speed wireless communication[1–3] and ultrafast computing.[4–6] Despite this urgent need, generation and detection of THz radiation remains a challenging task that pursues innovative approaches for its coherent control and optimization. With the surge in spintronic technologies in recent years, the ultrafast demagnetization[7] dynamics in these devices may enable the next generation of efficient THz emitters.[8–10] Spintronic THz emitters offer numerous advantages, including phase reversal upon the switching of the applied magnetic field[11] or pump direction, scalable and heavily researched production methods,[12] and versatility of pump wavelength.[13] The spintronic THz emitters consist of a spin current source, often a ferromagnet (FM), interfaced with a material, which can convert the spin current to a corresponding charge current through the inverse Rashba-Edelstein effect[9,14,15] or inverse spin Hall effect (ISHE).[8,16] More commonly, these materials are heavy metals with a large spin Hall angle θ_{SH}, but have recently been replaced with semiconductors and various 2D materials.[17–19] Upon an optical pump from a femtosecond laser pulse, hot carriers are generated in the ferromagnet (FM) layer, which constitute a spin-polarized current that propagates toward the interface and is injected into the adjacent material as shown in **Figure 1**A. As a result of this injected spin-polarized current, a transient electric dipole is formed through the ultrafast spin-to-charge (STC) conversion[20] process that results in THz radiation, with the electric field perpendicular to the spin polarization, described by the equation:

$$\vec{E}_{THz}(t) \propto P_S \theta_{SH} \vec{J}_S \times \vec{\sigma}_S \tag{1}$$

where $\vec{E}_{THz}(t)$ is the transient THz electric field generated in the nonmagnetic layer, $\vec{\sigma}_S$ and $\vec{J}_S$ is the unit vector of spin polarization direction and spin current density of the injected spin current from the FM layer upon ultrafast laser excitation, respectively. θ_{SH} is the STC conversion efficiency of the nonmagnetic layer that is proportional to the strength of the spin-orbit coupling or Rashba parameters.[15] P_S is the spin injection efficiency at the interface that is determined by the bandgap alignment between the ferromagnet and nonmagnetic material.[17] Therefore, there are two limiting factors at play determining the THz device performance; first is the spin polarization and injection efficiency at the interface, P_S that strongly depends on the bandgap of the semiconductor and

A. Comstock, M. Biliroglu, D. Seyitliyev, A. McConnell, E. Vetter, K. Gundogdu, D. Sun
Department of Physics and Organic and Carbon Electronics Lab (ORaCEL)
North Carolina State University
Raleigh, NC 27695, USA
E-mail: kgundog@ncsu.edu; dsun4@ncsu.edu

P. Reddy, R. Kirste, D. Szymanski
Adroit Materials, Inc.
2054 Kildaire Farm Rd., Cary, NC 27518, USA

Z. Sitar, R. Collazo
Department of Materials Science and Engineering
North Carolina State University
Raleigh, NC 27695, USA

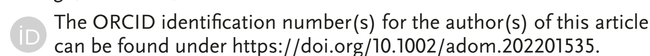
The ORCID identification number(s) for the author(s) of this article can be found under https://doi.org/10.1002/adom.202201535.

© 2022 The Authors. Advanced Optical Materials published by Wiley-VCH GmbH. This is an open access article under the terms of the Creative Commons Attribution License, which permits use, distribution and reproduction in any medium, provided the original work is properly cited.

DOI: 10.1002/adom.202201535

© 2022 The Authors. Advanced Optical Materials published by Wiley-VCH GmbH

21951071, 0, Downloaded from https://onlinelibrary.wiley.com/doi/10.1002/adom.202201535 by North Carolina State University, Wiley Online Library on [01/11/2022]. See the Terms and Conditions (https://onlinelibrary.wiley.com/terms-and-conditions) on Wiley Online Library for rules of use; OA articles are governed by the applicable Creative Commons License

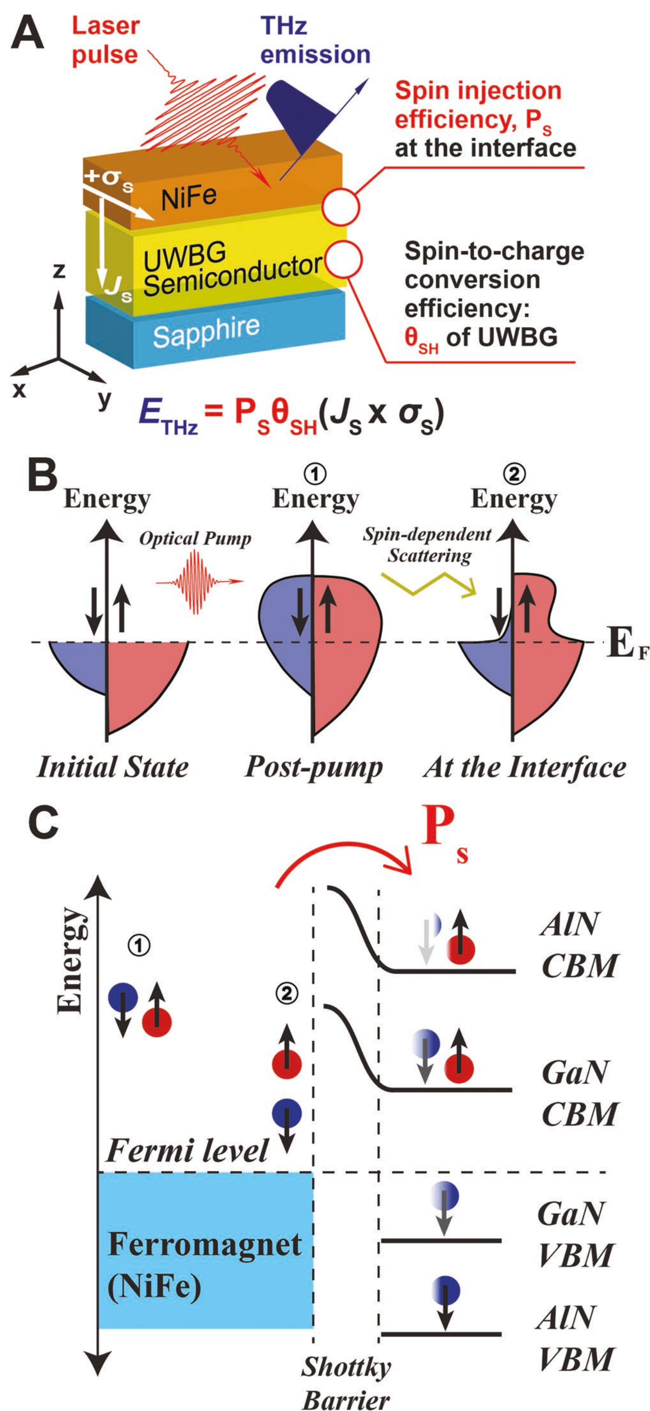

Figure 1. A) Schematic of spin injection from a ferromagnet into wide (GaN) and ultrawide (AlN) bandgap semiconductors under femtosecond laser excitation. The wide bandgap of AlN acts as a spin filter, which does not accept the lower energy, spin minority carriers. B) Shows the increased rate of thermalization of the minority carriers when the hot electrons reach the ferromagnet/semiconductor interface. C) Increased energy level of the spin majority (↑) and minority (↓) carriers immediately following the femtosecond laser pump. The Schottky barrier ensures that primarily the spin majority carriers enter the semiconductor, although the lower bandgap of GaN allows for more low-energy electrons to be injected, which reduces the overall spin polarization efficiency.

Schottky barrier, respectively,[17] and the second is the STC conversion efficiency. Through materials substitution and device engineering, we show that semiconducting heterostructures offer control and optimization of both of these factors to generate high-performance THz emitters .

First, we investigate the effects of the semiconducting band gap on the spin polarization at the interface. Figure 1B schematically depicts the interfacial energy level alignment of the spintronic device. After excitation by the femtosecond laser pulse, majority and minority spin-polarized electrons are generated in the FM layer (NiFe), constituting a superdiffusive spin current that propagates toward the interface with the adjacent material. Due to the asymmetry in scattering rates between these two carriers, the minority spin-polarized electrons will thermalize at a greater rate toward a Fermi-Dirac distribution, and will on average have lower energy[21] than the majority spin-polarized electrons. At the semiconducting interface, only the electrons with energy above the bandgap will tunnel into the semiconductor,[22] so the bandgap of the semiconductor acts as a spin filter, which increases the degree of spin polarization. In a similar way, the depletion region of the semiconductor will act as a tunneling barrier, allowing preferential transmission of the higher energy majority carriers and effectively tuning the spin injection efficiency.[17] This thermalization process is described in Figure 1C immediately after the laser excitation, and when the excited electrons reach the interface, after the spin-dependent scattering process. Based on this model, lower bandgap materials exhibiting lower Schottky barriers would accept more minority spin-polarized carriers, resulting in the limited degree of polarization of the spin current. We investigate these effects not only by substituting the WBG semiconductor GaN with an UWBG semiconductor AlN but by also doped AlN with *n*-type carriers to tune the conduction band minimum.

After the injection of the highly spin-polarized current, a STC conversion process takes place to convert the spin current into a charge current, which will result in electromagnetic radiation from the rapidly oscillating dipole.[23] This STC conversion may be due either to the bulk Rashba or inverse spin hall effect (ISHE), or the interfacial Rashba effect, which manifests in systems with broken inversion symmetry, such as two-dimensional electron gases (2DEGs).[15,24] In all-metallic systems, a nonmagnetic heavy metal such as Pt is often used to generate large charge currents. However, in most common semiconductors, the spin Hall angle θ_{SH} is relatively small. Therefore, recent interest has been sparked in the study of THz emission from interfacial Rashba states arising in 2DEG's, both for their enhanced STC conversion mechanisms,[9,14] as well as its control over asymmetric THz emission as induced by the polarization of the optical pump.[18] Following this motivation, we have also fabricated $Al_{0.25}Ga_{0.75}N$/GaN (AlGaN/GaN) heterostructures, which form a 2DEG at the interface and successfully demonstrated both enhanced and asymmetric THz emission from the interfacial Rashba state. Combined with the interface with the wider bandgap AlGaN exhibiting a larger barrier that acts as a spin filter and the 2DEG at the interface, we show that spintronic THz efficiency can be greatly increased.

© 2022 The Authors. Advanced Optical Materials published by Wiley-VCH GmbH

21951071, 0, Downloaded from https://onlinelibrary.wiley.com/doi/10.1002/adom.202201535 by North Carolina State University, Wiley Online Library on [01/11/2022]. See the Terms and Conditions (https://onlinelibrary.wiley.com/terms-and-conditions) on Wiley Online Library for rules of use; OA articles are governed by the applicable Creative Commons License

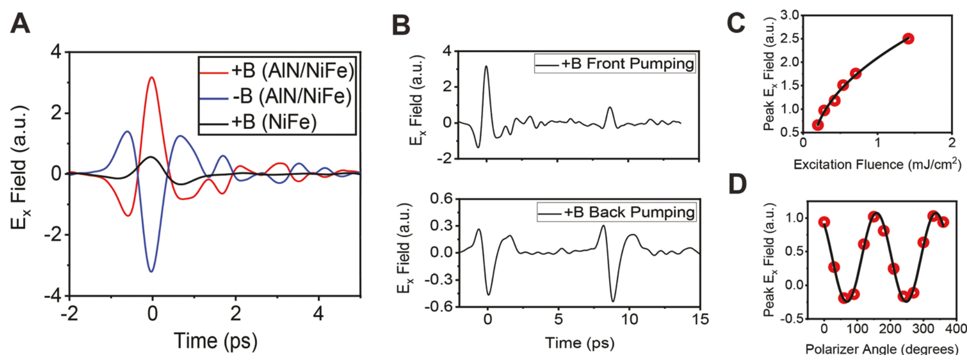

Figure 2. A) Spintronic THz emission from a heterostructure (AlN/NiFe) involving UWBG semiconductor, AlN. The signal changes its phase upon switching of the magnetic field, implying the spintronic origin of the observed emission. A reference NiFe sample is shown to demonstrate the enhancement of the observed radiation in the semiconducting device. B) THz emission under front and back incidence of the pump, where the phase of the THz signal is reversed. Secondary peaks are present that represent the reflection of spin current at the boundaries of the device. C) Square-root dependence of THz electric field strength corresponding with intensity being proportional to pump fluence. D) Linearly polarized THz emission shown in this plot confirms their spintronic nature.

2. Results and Discussion

2.1. Spintronic THz Emission from an UWBG Semiconductor

To study the effects of the bandgap on THz emission, NiFe (5 nm)/AlN (20 nm) heterostructures were fabricated on a sapphire substrate. AlN is an UWBG semiconductor (6.0 eV)[25] as opposed to previously studied GaN (3.4 eV)[19] or MoS_2 (1.9 eV).[17] The time-resolved THz electric field is measured as described in the Experimental Section. In **Figure 2**A, the waveform of the electric field emitted from the device is shown alongside the emission from a single NiFe only control device. Clear enhancement of the THz signal is seen in the bilayer structure over the single NiFe layer due to the STC conversion that occurs in the AlN due to bulk Rashba effects similar to GaN stemming from their noncentrosymmetric crystal structure.[26]

A series of control experiments were performed to confirm that the observed THz emission from the UWBG semiconductor is indeed spintronic in its origin. Figure 2A demonstrates that when the applied field is switched, the polarization of the THz field is reversed. This is direct evidence of the spintronic nature of the THz emission, because when the magnetization of the NiFe layer is reversed, the spin orientation of the majority and minority carriers also reverses, which changes both the direction of the transient charge current and electric field as shown in Equation (1). As a second test, we changed the incidence of the optical pump direction from the NiFe side (front pumping) to the sapphire side (back pumping). This inversion alters the direction of the spin current injection in the device and subsequently should switch the direction of the charge current, i.e., the phase of the radiated electric field.[27] The effects of pumping direction from both sides of the device are shown in Figure 2B. In these measurements, two clear peaks are observed corresponding to THz emission from two different incident directions. The first peak is from the emission of the direct superdiffusive spin current generated by the laser excitation, and the second peak is due to reflection of this spin current at the boundaries of the device with air that generates a secondary spin current, resulting in a delayed signal.[27] Power dependence on the pump excitation produces a sublinear response in the peak transmission amplitude shown in Figure 2C, indicating a square-root relationship between the power of the optical pump and the spin current generated from the NiFe as expected.[12] Moreover, a wire-grid polarizer was inserted between the THz emitter and detector, allowing for some insight into the degree of polarization of the pulse. A clear $\cos(2\theta)$ dependence is observed in Figure 2D, demonstrating that the THz emission is roughly linearly polarized, with the polarization axis perpendicular to the applied magnetic field direction, as would be expected for the STC conversion process.

2.2. Effects of Bandgap, Doping, and Polarity on THz Emission

We demonstrated in the previous section that the NiFe/AlN heterostructure produces spintronic THz emission as a result of the STC conversion. To test the effect of bandgap, we compare the THz emission intensity in undoped NiFe (5 nm)/AlN (20 nm) to that of NiFe/GaN measured previously.[19] The strength of both signals is normalized with respect to the same NiFe (5 nm)-only sample to be used as a control experiment that is measured at the same time. **Figure 3**A demonstrates that the total amplitude of the THz field is roughly 1.5x larger in the NiFe/AlN as compared with that in the NiFe/GaN heterostructure. This is consistent with the fact that the higher bandgap of AlN would result in a greater degree of spin polarization, P_S at the NiFe/AlN interface and thus a larger emission amplitude than GaN. This enhancement in THz field strength is understood in spite of the decreased STC conversion efficiency θ_{SH} in the AlN layer since it possesses a much weaker bulk spin-orbit coupling ($\propto Z^4$, where Z is an effective atomic number) compared with that of GaN. Moreover, considering the dominant role of broken inversion symmetry in a wurtzite crystal structure[28] that leads to the Rashba effect, the STC conversion in both compounds can be attributed to the inverse Rashba Edelstein effect (IREE) that is directly proportional to the Rashba parameter, α_R, i.e., $\theta_{SH} \approx \frac{1}{2}\lambda\frac{\alpha_R \tau_p}{\hbar}$, where λ is the effective spin diffusion length at the interface, τ_p is the momentum

© 2022 The Authors. Advanced Optical Materials published by Wiley-VCH GmbH
21951071, 0, Downloaded from https://onlinelibrary.wiley.com/doi/10.1002/adom.202201535 by North Carolina State University, Wiley Online Library on [01/11/2022]. See the Terms and Conditions (https://onlinelibrary.wiley.com/terms-and-conditions) on Wiley Online Library for rules of use; OA articles are governed by the applicable Creative Commons License

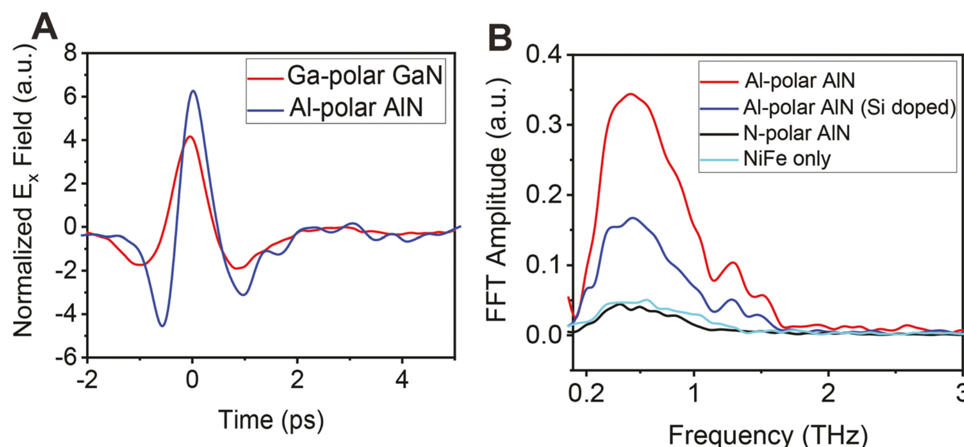

Figure 3. A) Comparison of THz waveforms from AlN (this work) and GaN (reproduced with permission from Ref. [19]) shows the enhanced THz emission in the AlN due to its larger spin polarization. These data have been normalized against a bare NiFe sample measured at the same time. B) Frequency domain signals generated from a couple of UWBG-based THz devices using Al-polar AlN (red), Si-doped Al-polar AlN (blue), and N-polar AlN (black). These data are also shown with a reference NiFe film (light blue).

scattering time, and ħ is the Planck constant.[15] Previous experimental studies show that the Rashba parameter in GaN (≈5 −10 meV Å)[29] is roughly one order of magnitude higher than that in the AlN-based compounds (< 1 meV Å).[29] Thus, we could estimate that the spin polarization injection efficiency P_S at the NiFe/AlN would be at least five times higher than that of the NiFe/GaN interface, strongly indicating that the efficient spin-filtering effect caused by the wider bandgap.

Next, we studied the impact of doping on spectral properties of spintronic THz emission from UWBG devices. Figure 3B shows the frequency-domain of the THz field measured in several UWBG semiconductor-based THz devices. Here, the emitted THz signal in the NiFe/AlN heterostructure contains a fast Fourier transform (FFT) components that persist up to 1.5-2 THz with the maximum occurring at about 0.5 THz. The bandwidth of THz emission is limited in part using the ZnTe crystal in the detection part of the setup. We found that the undoped AlN device exhibits a much stronger THz intensity compared with that in the Si-doped AlN device (carrier concentration: ≈5×10^{15} cm^{-3}). The observed carrier concentration dependence of the emission can be interpreted in the context of the spin-filtering effect at the interface. Because silicon doping introduces *n*-type carriers into the AlN, the Fermi level will be shifted to higher energy. However, when the interface is formed with the semiconductor and the NiFe, the Fermi level must be constant across the boundary. This causes the conduction band to shift to a lower energy, and thus accepting more carriers with a lower energy, i.e., minority spin-polarized electrons. This shift in the conduction band minimum reduces the overall injected spin-polarized current and THz amplitude, as previously discussed. One persisting question is that with the change of the elements that make up the semiconducting material, the spin Hall angle θ_{SH} could be changed. However, doping with silicon was used in that it has a similar atomic weight to Al, so its replacement of Al should not greatly affect the STC conversion in the semiconducting layer. Considering the technical difficulties in doping the UWBG materials, the pronounced spintronic THz emission in the undoped UWBG sample circumvents the current bottleneck problems and provides a promising route to realize the high-performance THz emitters.

Furthermore, the effects of the polarity (crystal orientation) on the THz generation are studied. By switching the structural polarity of the AlN layer from Al-polar to N-polar during the deposition, the THz amplitude is greatly reduced while interfacing with the same FM layer and shows almost no difference with the bare NiFe sample. This may be attributed to the piezoelectric effects of AlN, which constitutes an effective electric field normal to the plane of the sample and may inhibit the injection of spin-polarized electrons.[30] Alternatively, this pseudo-interfacial built-in electric field induced by the polarity may change the Rashba effect as demonstrated in the gate voltage-dependent STC conversion in the oxide heterostructures.[31] As a result, the interfacial atomic structure impacts the STC conversion via the inverse Rashba Edelstein effect and determines the resulting THz field generation.

2.3. Enhancement of THz Emission Amplitude using a 2DEG

Device configurations for spintronic THz emitters are enriched with semiconducting applications due to their well-studied fabrication methods for forming heterostructures with high-quality interfaces. Most notably, heterostructures involving the 2DEG have received recent attention for their applications in STC conversion mechanisms involving pronounced interfacial Rashba states, enabling on-demand control of THz emission.[9,14] Following this trend, we found it beneficial to study the THz emission from a NiFe (5 nm)/$Al_{0.25}Ga_{0.75}N$ (20 nm)/GaN (200 nm)/GaN (2 nm, buffer)/AlN (20 nm, nucleation)/Sapphire heterostructure as depicted in **Figure** 4A, where the 2DEG is formed at the AlGaN/GaN interface.[32] This device configuration offers a chance to realize a THz efficiency that triumphs over individual semiconducting materials by utilizing both large spin polarization of the injected spin current at the NiFe/AlGaN interface due to larger Schottky barrier[26] and an efficient STC conversion process at the interfacial Rashba state.[28] In this experiment, the polarization of spin current that

© 2022 The Authors. Advanced Optical Materials published by Wiley-VCH GmbH

21951071, 0, Downloaded from https://onlinelibrary.wiley.com/doi/10.1002/adom.202201535 by North Carolina State University, Wiley Online Library on [01/11/2022]. See the Terms and Conditions (https://onlinelibrary.wiley.com/terms-and-conditions) on Wiley Online Library for rules of use; OA articles are governed by the applicable Creative Commons License

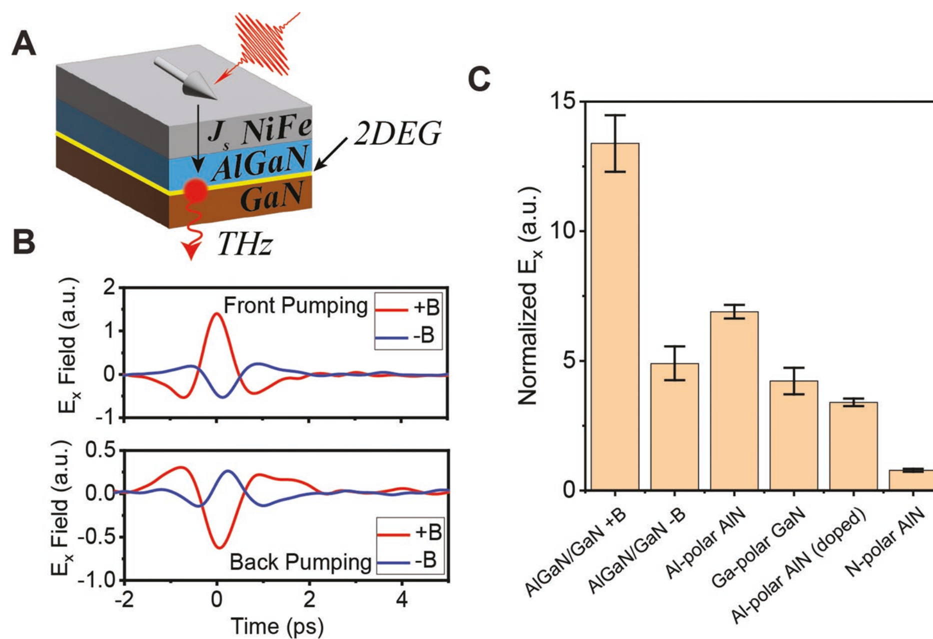

Figure 4. A) Schematic illustration of the spintronic THz emission from the NiFe/AlGaN/GaN heterostructure. Spin current injection from the NiFe is filtered by the AlGaN to enhance the spin polarization and impinges on the 2DEG between the AlGaN and GaN where an efficient STC conversion process takes place, resulting in the THz radiation. B) THz waveforms under front and back pumping with positive- and negative-applied fields to confirm the mechanisms responsible for the observed phenomenon. C) A summary of normalized THz amplitude from different UWBG-based spintronic THz emitters in this work.

is generated in the NiFe layer will be primarily enhanced by the wider bandgap of the AlGaN compared with GaN. Considering the relatively large spin diffusion length in the GaN-based materials (≈200 nm),[33] injected spin current will transmit across the entire AlGaN spacer layer while maintaining their high spin polarization degree and reach the 2DEG interface, where the primary STC conversion process occurs. However, it is noteworthy that this spin current may continue to diffuse to the GaN layer, not subject to any further spin-filtering mechanisms as the GaN bandgap is lower than the AlGaN bandgap. Since the GaN likely has a larger spin Hall angle than that of AlN (and thus AlGaN), an enhancement of the THz amplitude in this heterostructure may be present simply due to a combination of the AlGaN bandgap and the spin orbit coupling strength of GaN. Thus, it is crucial to confirm that the STC conversion occurs primarily at the Rashba interface that inside the bulk GaN layer.

Previous work has demonstrated that the Rashba interface may interact with the electric field of the optical pump to form an electric dipole moment, causing a shift of both of the spin-splitting sub-bands toward one direction in k-space, resulting in an asymmetric THz signal.[18] However, this effect will be only observed in the 2D case and cannot be seen due to the bulk Rashba states, which are present in the GaN or AlN alone. With the help of this unique feature, it would be straightforward to confirm that the THz emission in these trilayer structures is generated from the interfacial Rashba interface as supported by the asymmetric signals in Figure 4B. These asymmetric signals persist upon reversal of the applied pump direction and external field direction. In both cases, the emission for field along +B exhibits a larger amplitude. This is because when the device geometry was inverted to excite from the sapphire side, the direction of +B or the k-vector of the optical pump remain unchanged. The observed asymmetry in the emission amplitude is consistent with previous results, which focused on the gate-tunable STC conversion mechanisms in 2DEG's,[31] and opens the possibilities for coherent control over THz emission using UWBG semiconductor-based devices.

After confirmation of the THz emission from the interfacial AlGaN/GaN Rashba state, we therefore quantify the THz emission amplitude from a variety of Nitride-based semiconductors and heterostructures, normalizing the peak THz emission to that of a bare NiFe film on a sapphire substrate. The comparison between these normalized amplitudes is shown in Figure 4C. The NiFe/AlGaN/GaN sample exhibits the largest THz amplitude that is roughly two times larger than that from the NiFe (5 nm)/AlN (20 nm) sample. Our results are consistent with the model that we have discussed as it relates to the THz emission efficiency and provide clear evidence that the Rashba state, as well as the higher bandgap of AlGaN, may harmonize to boost the spintronic THz device performance.

3. Conclusion

Inspired by the enhanced fabrication techniques for high-quality semiconducting films and interfaces, as well as the rapidly expanding study of the replacement of the metallic components of conventional spintronic THz emitters, we systematically studied the effects of bandgap and STC conversion in the UWBG semiconductors on the spintronic THz generation efficiency. We found that by substituting AlN (E_g = 6.0 eV) for

© 2022 The Authors. Advanced Optical Materials published by Wiley-VCH GmbH
21951071, 0, Downloaded from https://onlinelibrary.wiley.com/doi/10.1002/adom.202201535 by North Carolina State University, Wiley Online Library on [01/11/2022]. See the Terms and Conditions (https://onlinelibrary.wiley.com/terms-and-conditions) on Wiley Online Library for rules of use; OA articles are governed by the applicable Creative Commons License

GaN (E_g = 3.4 eV) in a NiFe/semiconductor heterostructure, the bandgap increases the spin polarization injection while the reduced spin Hall angle in the AlN layer lowers the STC conversion efficiency by a smaller factor, resulting in the enhancement of overall THz intensity. To mitigate the decreased STC conversion while maintaining the high spin injection, the AlGaN/GaN heterostructure was employed, which incorporates both a large bandgap and the 2D Rashba interface for the large STC conversion, leading to the best performing THz device. Our work enables the design of UWBG semiconductor-based devices for future energy-efficient spintronic THz applications.

4. Experimental Section

Sample Fabrication: All *n*-AlN and AlGaN/GaN samples studied here were grown on sapphire substrates in a vertical, cold-walled, RF-heated, low-pressure metalorganic chemical vapor deposition (MOCVD) reactor. A 5-nm thick $Ni_{81}Fe_{19}$ layer was grown on top of the AlN and AlGaN/GaN layer by e-beam evaporation with a base pressure less than 1×10^{-6} Torr and a deposition rate of 0.25 Å s^{-1}. Rocking curves of GaN were 259 and 630 arcsecond in (002) and (302), respectively. The 2DEG density at the AlGaN/GaN interface was 1.1×10^{13} cm^{-2} with 1390 cm^2 V^{-1} s^{-1} mobility at room temperature. In order to verify the STC efficiency of the AlGaN/GaN heterostructure, λ_{IEE} is also calculated. Note that the Rashba parameter for AlGaN/GaN was $\alpha_R = 5 \times 10^{-13}$ eV · m[34] and the effective mass of the electrons in the interfacial 2DEG was $m_e^* = 0.285 m_e$.[35] The relaxation time was $\tau_p = \frac{\mu m_e^*}{e} = 2.25 \times 10^{-13}$ s; therefore, $\lambda_{IEE} = \frac{\alpha_R \tau_p}{\hbar} = 0.17$ nm.[31] This was consistent with STC values for other systems like NiFe/Pt (by considering, $\lambda_{IEE} \approx \theta_{SHE} \cdot \lambda_{Pt}$; $\theta_{SHE} = 0.1$ and $\lambda_{Pt} = 2$ nm of the Pt).

THz Measurement Setup: THz measurements were performed using the output of a 1 kHz repetition rate Ti:sapphire amplifier (Quantronix Integra-C). The central wavelength was 800 nm and pulse duration was 120 fs. The THz emission was electrically detected using a 1-mm thick [110] ZnTe crystal. A static magnetic field of 300 mT was applied for all measurements. A wire grid polarizer-oriented orthogonal to the magnetic field was used to collect the THz waveform and was rotated to analyze the polarization of the emitted signal in Figure 2. All measurements were performed at room temperature.

Supporting Information

Supporting Information is available from the Wiley Online Library or from the author.

Acknowledgements

A.C. and M.B. contributed equally to this work. D.S. acknowledges the support from National Science Foundation (grant No. ECCS-1933297). K.G. acknowledges the support from ROI from UNC system and National Science Foundation EFRI-NewLAW program (Grant No. 1741693). Z.S. and R.C. acknowledge the partial support from National Science Foundation (grant Nos. ECCS-1916800, ECCS-1610992, and ECCS-1653383), and by the Air Force Office of Scientific Research (AFOSR) (grant No. FA-95501710225).

Conflict of Interest

The authors declare no conflict of interest.

Data Availability Statement

The data that support the findings of this study are available from the corresponding author upon reasonable request.

Keywords

spintronics, terahertz, two-dimensional electron gas, ultrawide bandgap semiconductors

Received: July 1, 2022
Revised: September 7, 2022
Published online:

[1] H. Elayan, O. Amin, R. M. Shubair, M.-S. Alouini, in *2018 International Conference on Advanced Communication Technologies and Networking (CommNet)*, IEEE, Marrakech, Morocco **2018**, https://doi.org/10.1109/COMMNET.2018.8360286.
[2] Z. Chen, X. Ma, B. Zhang, Y. Zhang, Z. Niu, N. Kuang, W. Chen, L. Li, S. Li, *China Commun.* **2019**, *16*, 1.
[3] W. Hoppe, J. Weber, S. Tirpanci, O. Gueckstock, T. Kampfrath, G. Woltersdorf, *ACS Appl. Nano Mater.* **2021**, *4*, 7454.
[4] M. Tonouchi, *Nat. Photonics* **2007**, *1*, 97.
[5] S. S. Dhillon, M. S. Vitiello, E. H. Linfield, A. G. Davies, M. C. Hoffmann, J. Booske, C. Paoloni, M. Gensch, P. Weightman, G. P. Williams, E. Castro-Camus, D. R. S. Cumming, F. Simoens, I. Escorcia-Carranza, J. Grant, S. Lucyszyn, M. Kuwata-Gonokami, K. Konishi, M. Koch, C. A. Schmuttenmaer, T. L. Cocker, R. Huber, A. G. Markelz, Z. D. Taylor, V. P. Wallace, J. A. Zeitler, J. Sibik, T. M. Korter, B. Ellison, S. Rea, et al., *J. Phys. D: Appl. Phys.* **2017**, *50*, 043001.
[6] M. Tong, Y. Hu, W. He, S. Hu, X. Cheng, T. Jiang, *ACS Nano* **2022**, *16*, 8294.
[7] A. Eschenlohr, M. Battiato, P. Maldonado, N. Pontius, T. Kachel, K. Holldack, R. Mitzner, A. Föhlisch, P. M. Oppeneer, C. Stamm, *Nat. Mater.* **2013**, *12*, 332.
[8] T. Seifert, S. Jaiswal, U. Martens, J. Hannegan, L. Braun, P. Maldonado, F. Freimuth, A. Kronenberg, J. Henrizi, I. Radu, E. Beaurepaire, Y. Mokrousov, P. M. Oppeneer, M. Jourdan, G. Jakob, D. Turchinovich, L. M. Hayden, M. Wolf, M. Münzenberg, M. Kläui, T. Kampfrath, *Nat. Photonics* **2016**, *10*, 483.
[9] C. Zhou, Y. P. Liu, Z. Wang, S. J. Ma, M. W. Jia, R. Q. Wu, L. Zhou, W. Zhang, M. K. Liu, Y. Z. Wu, J. Qi, *Phys. Rev. Lett.* **2018**, *121*, 086801.
[10] P. Agarwal, L. Huang, S. Ter Lim, R. Singh, *Nat. Commun.* **2022**, *13*, 4072.
[11] T. Kampfrath, M. Battiato, P. Maldonado, G. Eilers, J. Nötzold, S. Mährlein, V. Zbarsky, F. Freimuth, Y. Mokrousov, S. Blügel, M. Wolf, I. Radu, P. M. Oppeneer, M. Münzenberg, *Nat. Nanotechnol.* **2013**, *8*, 256.
[12] T. S. Seifert, L. Cheng, Z. Wei, T. Kampfrath, J. Qi, *Appl. Phys. Lett.* **2022**, *120*, 180401.
[13] E. T. Papaioannou, G. Torosyan, S. Keller, L. Scheuer, M. Battiato, V. K. Mag-Usara, J. L'huillier, M. Tani, R. Beigang, *IEEE Trans. Magn.* **2018**, *54*, 9100205.
[14] M. B. Jungfleisch, Q. Zhang, W. Zhang, J. E. Pearson, R. D. Schaller, H. Wen, A. Hoffmann, *Phys. Rev. Lett.* **2018**, *120*, 207207.
[15] J. C. R. Sánchez, L. Vila, G. Desfonds, S. Gambarelli, J. P. Attané, J. M. De Teresa, C. Magén, A. Fert, *Nat. Commun.* **2013**, *4*, 2944.
[16] K. Ando, S. Takahashi, J. Ieda, Y. Kajiwara, H. Nakayama, T. Yoshino, K. Harii, Y. Fujikawa, M. Matsuo, S. Maekawa, E. Saitoh, *J. Appl. Phys.* **2011**, *109*, 103913.

© 2022 The Authors. Advanced Optical Materials published by Wiley-VCH GmbH

21951071, 0, Downloaded from https://onlinelibrary.wiley.com/doi/10.1002/adom.202201535 by North Carolina State University, Wiley Online Library on [01/11/2022]. See the Terms and Conditions (https://onlinelibrary.wiley.com/terms-and-conditions) on Wiley Online Library for rules of use; OA articles are governed by the applicable Creative Commons License

[17] L. Cheng, X. Wang, W. Yang, J. Chai, M. Yang, M. Chen, Y. Wu, X. Chen, D. Chi, K. E. J. Goh, J.-X. Zhu, H. Sun, S. Wang, J. C. W. Song, M. Battiato, H. Yang, E. E. M. Chia, *Nat. Phys.* **2019**, *15*, 347.
[18] K. Cong, E. Vetter, L. Yan, Y. Li, Q. Zhang, Y. Xiong, H. Qu, R. D. Schaller, A. Hoffmann, A. F. Kemper, Y. Yao, J. Wang, W. You, H. Wen, W. Zhang, D. Sun, *Nat. Commun.* **2021**, *12*, 5744.
[19] E. Vetter, M. Biliroglu, D. Seyitliyev, P. Reddy, R. Kirste, Z. Sitar, R. Collazo, K. Gundogdu, D. Sun, *Appl. Phys. Lett.* **2020**, *117*, 093502.
[20] E. Saitoh, M. Ueda, H. Miyajima, G. Tatara, *Appl. Phys. Lett.* **2006**, *88*, 182509.
[21] V. P. Zhukov, E. V. Chulkov, P. M. Echenique, *Phys. Rev. B* **2006**, *73*, 125105.
[22] M. Battiato, K. Held, *Phys. Rev. Lett.* **2016**, *116*, 196601.
[23] W. Wu, C. Yaw Ameyaw, M. F. Doty, M. B. Jungfleisch, *J. Appl. Phys.* **2021**, *130*, 091101.
[24] X. Zhang, N. Tang, L. Yang, C. Fang, C. Wan, X. Liu, S. Zhang, Y. Zhang, X. Wang, Y. Lu, W. Ge, X. Han, B. Shen, *Adv. Funct. Mater.* **2021**, *31*, 2009771.
[25] M. Feneberg, R. A. R. Leute, B. Neuschl, K. Thonke, M. Bickermann, *Phys. Rev. B* **2010**, *82*, 075208.
[26] W. Weber, S. D. Ganichev, S. N. Danilov, D. Weiss, W. Prettl, Z. D. Kvon, V. V. Bel'kov, L. E. Golub, H.-I. Cho, J.-H. Lee, *Appl. Phys. Lett.* **2005**, *87*, 262106.
[27] G. Torosyan, S. Keller, L. Scheuer, R. Beigang, E. T. Papaioannou, *Sci. Rep.* **2018**, *8*, 1311.
[28] W. Stefanowicz, R. Adhikari, T. Andrearczyk, B. Faina, M. Sawicki, J. A. Majewski, T. Dietl, A. Bonanni, *Phys. Rev. B* **2014**, *89*, 205201.
[29] R. Adhikari, M. Matzer, A. T. Martín-Luengo, M. C. Scharber, A. Bonanni, *Phys. Rev. B* **2016**, *94*, 085205.
[30] N. Thillosen, S. Cabañas, N. Kaluza, V. A. Guzenko, H. Hardtdegen, Th. Schäpers, *Phys. Rev. B* **2006**, *73*, 241311.
[31] E. Lesne, Y. Fu, S. Oyarzun, J. C. Rojas-Sánchez, D. C. Vaz, H. Naganuma, G. Sicoli, J.-P. Attané, M. Jamet, E. Jacquet, J.-M. George, A. Barthélémy, H. Jaffrès, A. Fert, M. Bibes, L. Vila, *Nat. Mater.* **2016**, *15*, 1261.
[32] J. P. Ibbetson, P. T. Fini, K. D. Ness, S. P. DenBaars, J. S. Speck, U. K. Mishra, *Appl. Phys. Lett.* **2000**, *77*, 250.
[33] S. Jahangir, F. Doğan, H. Kum, A. Manchon, P. Bhattacharya, *Phys. Rev. B* **2012**, *86*, 035315.
[34] H. Cheng, N. Biyikli, Ü. Özgür, Ç. Kurdak, H. Morkoç, V. I. Litvinov, *Physica E* **2008**, *40*, 1586.
[35] M. Li, Z. B. Zhao, L. B. Fan, *Phys. Scr.* **2014**, *90*, 015806.

© 2022 The Authors. Advanced Optical Materials published by Wiley-VCH GmbH

21951071, 0, Downloaded from https://onlinelibrary.wiley.com/doi/10.1002/adom.202201535 by North Carolina State University, Wiley Online Library on [01/11/2022]. See the Terms and Conditions (https://onlinelibrary.wiley.com/terms-and-conditions) on Wiley Online Library for rules of use; OA articles are governed by the applicable Creative Commons License